PVDIS Supplemental Material - Measurement of the Parity Violating Deep Inelastic Asymmetry and Extraction of the Quark Weak Axial Charge

D. Wang,[1] K. Pan,[2] R. Subedi,[1] X. Deng,[1] Z. Ahmed,[4] K. Allada,[5]
K. A. Aniol,[6] D. S. Armstrong,[7] J. Arrington,[8] V. Bellini,[9] R. Beminiwattha,[10]
J. Benesch,[11] F. Benmokhtar,[12] A. Camsonne,[11] M. Canan,[13] G. D. Cates,[1]
J.-P. Chen,[11] E. Chudakov,[11] E. Cisbani,[14] M. M. Dalton,[1] C. W. de Jager,[11,1]
R. De Leo,[15] W. Deconinck,[7] A. Deur,[11] C. Dutta,[5] L. El Fassi,[8] D. Flay,[16]
G. B. Franklin,[12] M. Friend,[12] S. Frullani,[14] F. Garibaldi,[14] A. Giusa,[9]
A. Glamazdin,[17] S. Golge,[13] K. Grimm,[18] K. Hafidi,[8] O. Hansen,[11] D. W. Higinbotham,[11]
R. Holmes,[4] T. Holmstrom,[19] R. Holt,[8] J. Huang,[2] C. E. Hyde,[13,20] C. M. Jen,[4]
D. Jones,[1] H. Kang,[21] P. King,[10] S. Kowalski,[2] K. S. Kumar,[22] J. H. Lee,[7,10]
J. J. LeRose,[11] N. Liyanage,[1] E. Long,[23] D. McNulty,[22] D. Margaziotis,[6] F. Meddi,[14]
D. G. Meekins,[11] L. Mercado,[22] Z.-E. Meziani,[16] R. Michaels,[11] M. Mihovilovic,[24]
N. Muangma,[2] K. E. Myers,[4] S. Nanda,[11] A. Narayan,[25] V. Nelyubin,[1] Nuruzzaman,[25]
Y. Oh,[21] D. Parno,[12] K. D. Paschke,[1] S. K. Phillips,[26] X. Qian,[27]
Y. Qiang,[27] B. Quinn,[12] A. Rakhman,[4] P. E. Reimer,[8] K. Rider,[19] S. Riordan,[1]
J. Roche,[10] J. Rubin,[8] G. Russo,[9] K. Saenboonruang,[1] A. Saha,[11], †, B. Sawatzky,[11]
A. Shahinyan,[11] R. Silwal,[1] S. Sirca,[24] P. A. Souder,[4] R. Suleiman,[11] V. Sulkosky,[2]
C. M. Sutera,[9] W. A. Tobias,[1] B. Waidyawansa,[10] B. Wojtsekhowski,[11] L. Ye,[28] B. Zhao,[7]
X. Zheng,[1,*]

[1]University of Virginia, Charlottesville, Virginia 22904, USA
[2]Massachesetts Institute of Technology, Cambridge, MA 02139, USA
[3]George Washington University, Washington, District of Columbia 20052, USA
[4]Syracuse University, Syracuse, New York 13244, USA
[5]University of Kentucky, Lexington, Kentucky 40506, USA
[6]California State University, Los Angeles, Los Angeles, California 90032, USA
[7]College of William and Mary, Williamsburg, Virginia 23187, USA
[8]Physics Division, Argonne National Laboratory, Argonne, Illinois 60439, USA
[9]Istituto Nazionale di Fisica Nucleare, Dipt. di Fisica dell'Univ. di Catania, I-95123 Catania, Italy
[10]Ohio University, Athens, Ohio 45701, USA
[11]Thomas Jefferson National Accelerator Facility, Newport News, Virginia 23606, USA
[12]Carnegie Mellon University, Pittsburgh, Pennsylvania 15213, USA
[13]Old Dominion University, Norfolk, Virginia 23529, USA
[14]INFN, Sezione di Roma, gruppo Sanità and Istituto Superiore di Sanità, I-00161 Rome, Italy
[15]Università di Bari, I-70126 Bari, Italy
[16]Temple University, Philadelphia, Pennsylvania 19122, USA
[17]Kharkov Institute of Physics and Technology, Kharkov 61108, Ukraine
[18]Louisiana Technical University, Ruston, Louisiana 71272, USA
[19]Longwood University, Farmville, Virginia 23909, USA
[20]Clermont Université, Université Blaise Pascal, CNRS/IN2P3, Laboratoire de Physique Corpusculaire, FR-63000 Clermont-Ferrand, France
[21]Seoul National University, Seoul 151-742, South Korea
[22]University of Massachusetts Amherst, Amherst, Massachusetts 01003, USA
[23]Kent State University, Kent, Ohio 44242, USA
[24]Institut Jožef Stefan, 3000 SI-1001 Ljubljana, Slovenia
[25]Mississippi State University, Starkeville, Mississippi 39762, USA
[26]University of New Hampshire, Durham, New Hampshire 03824, USA
[27]Duke University, Durham, North Carolina 27708, USA
[28]China Institute of Atomic Energy, Beijing, 102413, P. R. China

[†]Deceased [*]To whom correspondence should be addressed; E-mail: xiaochao@jlab.org

In this document we provide supplemental material in support of ... ...

1 PVDIS Formalism

This section discusses the formalism of parity-violating deep inelastic scattering. Extraction of the C_2 coefficients (section **??**) follow from this formalism.

$$A_{PV} \equiv \frac{\sigma_+ - \sigma_-}{\sigma_+ + \sigma_-} = \left(-\frac{G_F Q^2}{4\sqrt{2}\pi\alpha}\right)\left(2g_A^e Y_1 \frac{F_1^{\gamma Z}}{F_1^\gamma} + g_V^e Y_3 \frac{F_3^{\gamma Z}}{F_1^\gamma}\right) , \tag{1}$$

where Q^2 is the negative of the four-momentum transfer squared, G_F is the Fermi weak coupling constant, α is the fine structure constant, Y_1 and Y_3 are kinematic factors, and x is the Bjorken scaling variable. In the quark parton model,

$$F_1^{\gamma Z} = \sum g_V^q Q_q \left[q(x) + \bar{q}(x)\right] \tag{2}$$

$$F_3^{\gamma Z} = \sum g_A^q Q_q \left[q(x) - \bar{q}(x)\right] \tag{3}$$

$$F_1^{\gamma} = \frac{1}{2}\sum Q_q^2 \left[q(x) + \bar{q}(x)\right] \tag{4}$$

where Q_q is the electric charge of quarks and $q(x), \bar{q}(x)$ are quark distribution functions. Rewriting $g^e_{A(V)} g^q_{V(A)}$ as $C_{1(2)q}$, and assuming $R^\gamma = R^{\gamma Z} = 0$, one has $Y_1 = 1$ and

$$A_{PV} = \left(\frac{3 G_F Q^2}{\pi\alpha^2\sqrt{2}}\right) \times \frac{2C_{1u}[1 + R_C(x)] - C_{1d}[1 + R_S(x)] + Y_3(2C_{2u} - C_{2d})R_V(x)}{5 + R_S(x) + 4R_C(x)} , \tag{5}$$

where $R_{V,C,S}$ are related to quark distributions. The magnitude of the asymmetry is in the order of 10^{-4}, or 10^2 parts per million (ppm) at $Q^2 = 1$ (GeV/c)^2.

The tree-level Standard Model effective weak coupling constants $C_{1,2q}$ are

$$C_{1u} = 2g_A^e g_V^u = -\frac{1}{2} + \frac{3}{4}\sin^2\theta_W , \qquad C_{2u} = 2g_V^e g_A^u = -\frac{1}{2} + 2\sin^2\theta_W ,$$
$$C_{1d} = 2g_A^e g_V^d = \frac{1}{2} - \frac{2}{3}\sin^2\theta_W , \qquad C_{2d} = 2g_V^e g_A^d = \frac{1}{2} - 2\sin^2\theta_W ,$$

with θ_W the weak mixing angle. The goal of JLab E08-011 is to measure the PVDIS asymmetries to a statistical precision of 3% for the $Q^2 = 1.1\mathrm{GeV}^2$ point and 4% for the the $Q^2 = 1.9\mathrm{GeV}^2$ point. In addition, the systematic uncertainty goal is $< 3\%$, and under the assumption that hadronic physics corrections are small, our goal is to extract from these asymmetries the effective coupling constant combination $(2C_{2u} - C_{2d})$. The magnitude of the asymmetries is expected to be 90 and 170 ppm for the two measured kinematics of $Q^2 = 1.1$ and 1.9 (GeV/c)^2, respectively. To achieve the required precision, event rates up to 500 kHz are expected. Although this is not the first time the PVDIS asymmetries are measured, the only preceeding PVDIS measurement was carried out at SLAC (**?**, **?**) about 35 years ago, with a $\approx 9\%$ statistical and a $\approx 9\%$ systematic uncertainties. The increased precision of this experiment required better controls of all systematic uncertainties.

2 Apparatus

2.1 Polarized Electron Beam

2.2 Data Selection

Loose requirements were imposed on beam quality, removing periods of beam intensity, position, or energy instability, removing about 25% of the total data sample. No spin-direction-dependent cuts were applied. The dominant source of noise due to the beam arose from fluctuations in the beam current and beam energy.

As explained in detail in (**?**, **?**, **?**), the window-to-window differences in the asymmetry from beam jitter were reduced by using the correlations to beam position differences from precision beam position monitors, Δx_i by defining a correction $A_{beam} = \sum c_i \Delta x_i$. The c_i were measured several times each hour from calibration data where the beam was modulated using steering coils and an accelerating cavity. The largest c_i was for ^{208}Pb and was on the order of 50 ppb/nm. The spread in the resulting $A_n^m = A_{raw} - A_{beam}$ was observed to be dominated by counting statistics.

2.3 Pedestals and Linearity

The signals produced by the beam monitors and the detectors ideally are proportional to the actual rates in those devices. In reality, however, these signals can deviate from linearity over the full dynamic range and in general do not extrapolate to a zero pedestal.

To study the linearity of the detectors and cavity monitors, we compared them to an Unser monitor (***?***), a parametric current transformer which can be used as an absolute reference of current. For our purposes the Unser monitor's advantage is its excellent linearity at low currents which allows us to obtain the cavity monitor pedestals. However, the fluctuations in the Unser monitor's pedestals, which drift significantly on a time scale of several minutes, and the ordinarily small range of beam currents limited the precision of such comparisons during production data taking. Instead, we use calibration data in which the beam current is ramped up and down from zero to more than 50 μA. One cycle takes about a minute. The result is that for any given beam current we have about sixty samples spread over a half hour run. This breaks any random correlation between Unser pedestal fluctuations and beam current and converts the Unser pedestal systematic to a random error.

In order to study linearity, we make scatterplots of one signal versus another and fit each scatterplot to a straight line, using only events where $24\ \mu\mathrm{A} < I_1 < 34\ \mu\mathrm{A}$, a range in which exploratory fits suggested everything was fairly linear. We then examine the residuals between the scatterplots and the fits, relative to the signal size corresponding to about 32 μA, over the full range of beam current.

Figures 1 to 2 show the results as a function of I_1. In Fig. 1 we see the behavior of the two cavity monitors relative to the Unser monitor. Both show deviations from linearity below about 14 μA and above about 47 μA, though the high-current problem for I_1 is not as clear-cut as for

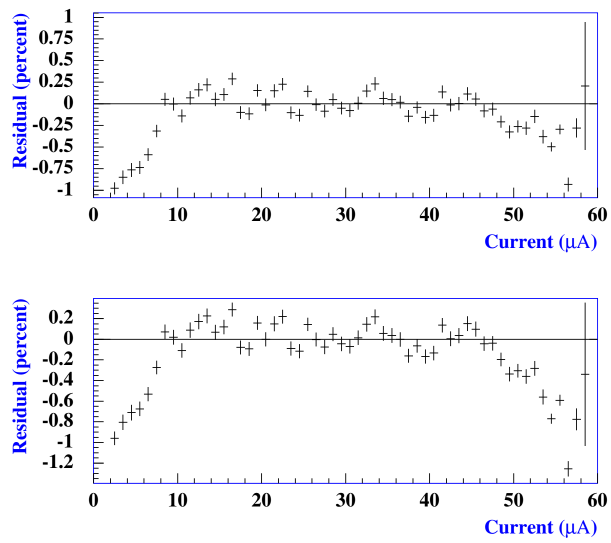

Figure 1: (Color online) (top) Residuals from fit of BCM1 to Unser data, as a fraction of the BCM1 pulse height at 32 μA, versus beam current. (bottom) Same for fit of BCM2 to Unser.

I_2 and the nonlinearities are at worst about 1% of the signal.

In Fig. 2 we see residuals for fits of the two detector signals versus I_1. The nonlinear behavior at low current is due mainly to the cavity monitors. From 32 μA to over 50 μA the detectors are linear to well under 0.2%.

We may conclude that the detectors and cavity monitors are linear to well within the required tolerances.

Detector pedestals were measured by averaging the detector signals during times when the beam is off. The resulting pedestals were always less than 0.3% of the signal corresponding to the lowest stable beam current in the production data set, and typically less than 0.06%; these pedestals are negligible.

The cavity monitor pedestals cannot be measured this way, since the cavity signals are mean-

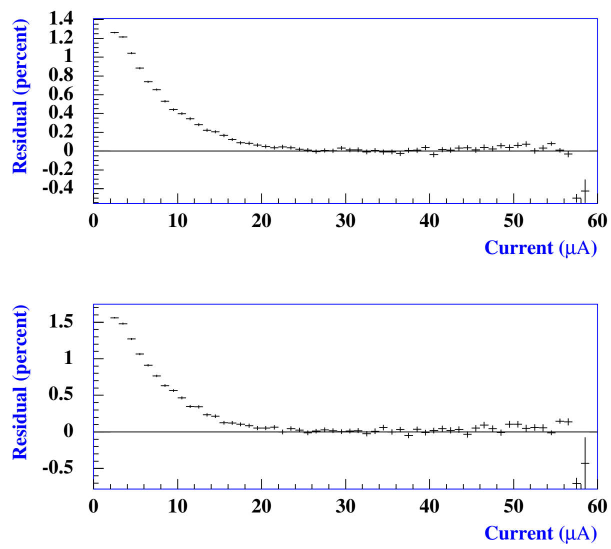

Figure 2: (Color online) (top) Residuals from fit of detector 1 to BCM1 data, as a fraction of the detector 1 pulse height at 32 μA, versus beam current. (bottom) Same for fit of detector 2 to BCM1.

ingless when the beam is off. Instead, we fit $I_{1(2)}$ to I_U in the calibration data and extrapolate to zero current. Such an extrapolation requires knowledge of the average Unser pedestal, which is obtained from the beam-off data in the same run. The resulting pedestals are less than 2% of the signal corresponding to the lowest stable beam current in the production data set.

In conclusion, no corrections for pedestals or nonlinearities needed to be applied. The nonlinearities of the detectors and cavity monitors were negligible over the dynamic range of the beam current we ran. The pedestals for detectors and cavity monitors were negligible.

2.4 Background Analysis

2.4.1 Target EndCap Correction

Scattering from the target aluminum windows contributed $(0.5 \pm 0.1)\%$ (???) to our detected signal. This background was measured by inserting into the beam an empty aluminum target cell, similar to the one used to contain liquid deuterium, and measuring the signal in our detector. The thickness of the empty target cell walls is about 10 times that of the walls used in the deuterium cell, in order to compensate for the radiative losses in the deuterium cell.

The correction to our data arises from ... ??? ... explain the physics here; I guess if it's DIS it's then Aluminum is not much different from Deuterium ...

2.4.2 Calibration of The HRS Optics

To calibrate the transfer matrix for the HRS, a 0.5 mm thick tungsten plate with an array of pinholes is inserted about 1 meter after the target and upstream of the first quadrupole of the HRS. The calibrations are dedicated runs at low rates with the vertical drift chambers (VDCs) turned on. Using the hole-pattern observed in the HRS focal plane, a chi-square minimization algorithm is performed to determine the matrix elements which transform the track vector to the location of the sieve slit.

Show some results from Kai Pan's analysis here.

2.4.3 Reconstruction of Q^2 and x

The four-momentum transfer squared is

$$Q^2 \;=\; 2\,E\,E'\,(1-\cos(\theta)) \tag{6}$$

where E is the incident energy, E' is the final momentum or energy of the electron ($E' \gg m_e$) and θ is the scattering angle.

For the beam energy we used the Tiefenbach energy (need to explain this) of ??? GeV and assumed a 3 MeV (???) average energy loss to the center of the target which is applied this as a correction to the beam energy. The error in the beam energy E and E' are assumed conservatively to be 3 MeV based on a history of these measurements in Hall A. The most important error is in θ ...

Perhaps need a table of errors.

2.5 Simulation

Two simulation packages were used to support the analysis of this experiment. The package called "hamc" (Hall A Monte Carlo) was used to simulate the events and the spectrometer acceptance, while a second package called "hats" (Hall A Trigger Simulation) was used to simulate the response of the trigger used to identify electrons and pions, providing a calculation of our deadtime.

In "hamc", events are generated using a physics class that has information about the cross section and asymmetry. The tracks are generated uniformly in solid angle $d\Omega = sin(\theta)\,d\theta\,d\phi$ and the results later weighted by the differential cross section $\frac{d\sigma}{d\Omega}$. The simulated tracks undergo multiple scattering in the target and energy loss from the target from external and internal Brehmstrahlung as well as ionization loss,

The generated four-vectors are transported to the detector in the HRS focal plane using a set of polynomials that model the trajectories of electrons through the magnetic fields. The beam raster is simulated, which produces a smearing of the beam on target. The events are transported to intermediate apertures such as the collimator or the entrance to quadrupoles. Events that reach the HRS focal plane and intersect the detectors are integrated to compute the total rate and average asymmetry.

Here describe “hats” ...

1. We would like to thank the personnel of Jefferson Lab for their efforts which resulted in the successful completion of the experiment. We thank T.-S.H. Lee, M. Gorshteyn, P. Blunden, A. Afanasev, J. Erler and their collaborators for carrying out the calculations used in this publication (list all theorists not co-author-ed here). X. Zheng would like to thank the Medium Energy Physics Group at the Argonne National Lab for supporting her during the initial work of this experiment. This work was supported by the Department of Energy (DOE), the National Science Foundation, and the Jeffress Memorial Trust. Jefferson Science Associates, LLC, operates Jefferson Lab for the U.S. DOE under U.S. DOE contract DE-AC05-060R23177.